THE ASTROPHYSICAL JOURNAL, 470:513–520, 1996 October 10

ROSAT OBSERVATIONS OF THE SOFT GAMMA-RAY BURST ERROR BOX COINCIDENT WITH THE SUPERNOVA REMNANT N49

D. MARSDEN, R. E. ROTHSCHILD, R. E. LINGENFELTER, AND R. C. PUETTER
Center for Astrophysics and Space Sciences 0111, University of California at San Diego, La Jolla, CA 92093-0111
Received 1995 December 1; accepted 1996 May 2

ABSTRACT

The supernova remnant N49 in the Large Magellanic Cloud was observed in soft X-rays using the High Resolution Imager aboard the *ROSAT* satellite. A total 0.1–2.4 keV image of the nebula was obtained by the use of a pixon-based image deconvolution algorithm. Image analysis determined the position of the X-ray hot spot (RX J05260.3−660433) coincident with the error box of the soft gamma-ray repeater SGR 0525−66. The position is R.A. (J2000) = $5^h26^m0^s.31$ and decl. (J2000) = $-66°4'33''.20$ with an uncertainty of 5″ in radius, due almost entirely to the *ROSAT* pointing uncertainty. This positional uncertainty is a factor of 2 smaller than that obtained from previous data. Examinations of optical images of N49 show no stellar sources coincident with the X-ray position of RX J05260.3−660433, with an upper limit of $m_V \sim 21$ mag. We have searched for periodicity in the signal from RX J05260.3−660433 in the period range 7.5–8.5 s, the approximate period observed from this source during the 1979 March 5 gamma-ray burst. No evidence for ∼8 s periodicity was found, and the upper limit on the pulsed fraction was determined to be 66%, for pulse profiles typical of X-ray pulsars. The overall counting rate from the hot spot was consistent with a constant signal over the ∼2 yr duration of the *ROSAT* observations.

Subject headings: gamma rays: bursts — ISM: individual (SNR N49) — Magellanic Clouds — pulsars: general — X-rays: ISM

1. INTRODUCTION

One of the most vexing problems in high-energy astrophysics is the origin of gamma-ray bursts (GRBs), bursts of high-energy radiation that seemingly emanate from random directions in the sky. Soft gamma-ray repeaters (SGRs) are a possible subclass of classical gamma-ray bursts that exhibit relatively soft spectra, generally short durations, and an apparent lack of spectral evolution (Norris et al. 1991; Rothschild 1995). All three of the known SGRs have been tentatively associated with supernova remnants: SGR 0526−66 with N49 (Cline et al. 1982), SGR 1806−20 with the Galactic supernova remnant G10.0−0.3 (Kulkarni & Frail 1993), and SGR 1900+14 with G42.8+0.6 (Vasisht et al. 1994). This suggests that the SGR bursts may come from the young (less than 10^4 yr) neutron stars formed during the supernova explosions responsible for the associated supernova remnant. This conclusion is bolstered by the observation of an X-ray point source coincident with the radio peak of G10.0−0.3 and the locus of a hard X-ray burst from SGR 1806−20 (Tanaka 1993), and the observation X-ray point sources coincident with the error boxes of SGR 1900+14 (Vasisht et al. 1994) and SGR 0526−66 (Rothschild, Kulkarni, & Lingenfelter 1994). Characteristics of the 1979 March 5 outburst of SGR 0526−66 (Mazets et al. 1979) also indicate a neutron star origin for this event. The short (0.2 ms) rise time, implying a maximum source size of 60 km, 8.0 ± 0.05 s pulsations, and a possible redshifted 511 keV emission line are all consistent with surface emission from a neutron star.

The large fluence and sharp time profile of the March 5 event allowed its position to be determined to an unprecedented accuracy through arrival time comparison between gamma-ray instruments on board a network of interplanetary spacecraft (Cline et al. 1982). The 0.09 arcmin^2 error box of this event fell inside the supernova remnant N49 in the Large Magellanic Cloud, a 5400 yr remnant (Vancura et al. 1992) located at a distance of 49 kpc (Feast 1991). Previous observations of N49 in soft X-rays by *Einstein* (Rothschild et al. 1993) and by *ROSAT* (Rothschild et al. 1994) revealed a pointlike "hot spot" consistent with the error box of SGR 0526−66, and the latter authors speculated that the X-ray emission from the hot spot could be attributed to the synchrotron nebula surrounding a young pulsar or to a peculiar binary system such as Circinus X-1. In the former case the energy source for the hot-spot emission could be either the steady spindown luminosity of the suspected pulsar or particles ejected from the SGR bursts themselves (Harding 1995). Alternatively, the ∼8 s pulsations seen during the 1979 March 5 burst have been generally ascribed to the rotation of a neutron star, possibly with a surface magnetic field of as much as $\sim 10^{14}$–10^{15} G (Duncan & Thompson 1992). To confound matters further, a ∼23 ms quasi-periodic oscillation was also detected during the 200 ms impulsive phase of the March 5 gamma-ray burst (Barat et al. 1983), although at a lesser significance than the 8 s periodicity.

Searches for counterparts to the quiescent X-ray source associated with SGR 0525−66 at other wavelengths have not revealed any convincing associations. The most recent such work (Dickel et al. 1995) used the X-ray hot-spot position from Rothschild et al. (1994) to place 3 σ upper limits on the radio (less than 0.3 Jy at 12.6 cm), infrared (less than 3.9×10^{-5} Jy and less than 5.8×10^{-5} Jy at 2.16 and 1.64 μm, respectively), and optical (less than 4×10^{-5} Jy at 656.3 nm) emission from the X-ray source in the SGR 0525−66 error box.

2. IMAGE ANALYSIS

The supernova remnant N49 was observed in the 0.1–2.4 keV band of the High Resolution Imager (HRI) on board the *ROSAT* satellite on four occasions between 1992 March 17 and 1994 January 5. The observations consisted of four

TABLE 1

THE FOUR *ROSAT* OBSERVATIONS OF N49

Observation	Start Date	End Date	Livetime (s)	N49 (counts s^{-1})	RX J0526 (counts s^{-1})
A[a]	1992 Mar 17	1992 Mar 21	21000	0.815 ± 0.006	0.016 ± 0.002
B	1992 Oct 22	1992 Nov 27	8170	0.808 ± 0.010	0.017 ± 0.003
C	1993 Feb 19	1993 Mar 19	12980	0.822 ± 0.008	0.018 ± 0.002
D	1994 Jan 05	1994 Jan 05	7535	0.792 ± 0.011	0.012 ± 0.003

[a] Same data set used by Rothschild et al. 1994.

separate observations with a total live time of just under 5×10^4 s (Table 1).

A reconstructed image of N49 was obtained by use of a pixon-based algorithm (Puetter 1994). The chief advantage of pixon algorithms over other restoration methods lies in the fact that they are multiresolution techniques in which the fitting process is constrained by the signal-to-noise ratio in each part of the data. Areas of the data with large signal-to-noise ratios are deconvolved on finer spatial scales than regions with a paucity of counts. This method avoids the introduction of spurious features in areas of the image with small numbers of counts. Pixon-based methods have been successful elsewhere in the deconvolution of the point-spread response function of the detector and the counting noise from images with low signal-to-noise ratios (Dixon et al. 1996). The total *ROSAT* image of N49 was deconvolved to produce the final image shown in Figure 1 with the SGR 0525−66 error box overplotted. The point source "hot spot" (RX J05260.3−660433) is clearly seen in the northern portion of the remnant, along with a broad, more elongated feature in the southeast.

To check the veracity of the deconvolved image, we performed separate image deconvolutions of the data: one in which the algorithm was unconstrained by the local signal-to-noise, and one in which the local smoothing scales were increased by a small but significant amount. The image obtained in the former case was a perfect fit to the data in the sense of maximizing the goodness-of-fit criterion, but as expected contained spurious features due to the overresolution of the data in regions of the image with sparse numbers of counts. The residuals in this case were flat and appeared spatially uncorrelated. The image produced in the latter case was a slightly worse fit to the data, and the residuals contained spatial correlations on scales similar to the smallest smoothing scale used. The image shown in Figure 1 produced residuals that were nearly identical numerically and spatially to the residuals from the unconstrained reconstruction and were free of the spatial correlations that resulted from using larger smoothing scales. The residuals of both the unconstrained and the pixon reconstruction (Fig. 1 image) are shown plotted in Figure 2. We conclude that the image in Figure 1 is an ideal reconstruction of the data in the sense that it uses the largest smoothing scales possible in producing a fit to the data that is as good as the unconstrained fit.

To locate the center of the hot-spot point source, the raw image was first smoothed with a Gaussian point-spread function of FWHM 5″. Then a section of the resulting image including the hot spot was fitted to a model consisting of a two dimensional Gaussian superimposed on sloping planar background. The fitted position for the hot-spot centroid was R.A. (J2000) = $5^h26^m0^s.31$ and decl. (J2000) = −66°4′33″.20, with the 1 σ fitting error being much less than the *ROSAT* positional (pointing) uncertainty of 5″. This error is a factor of 2 less than that obtained by Rothschild et al. (1994). Following the *ROSAT* naming convention for serendipitous sources, we give the point source the name RX J05260.3−660433. The excess

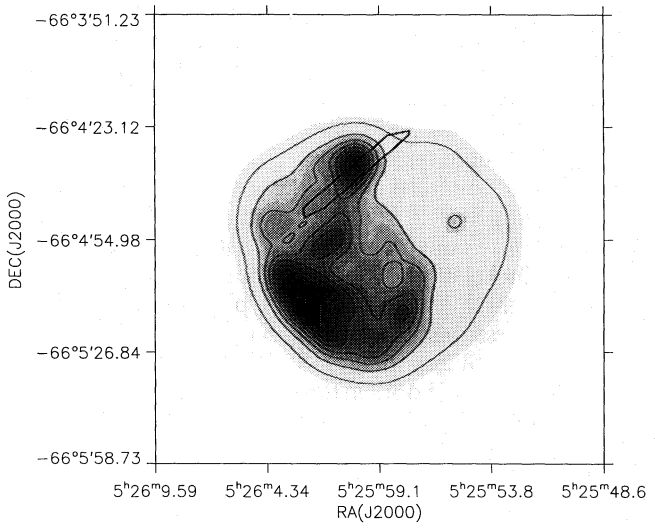

FIG. 1.—Reconstructed image of N49 obtained from the fractal pixon deconvolution of the total *ROSAT* High Resolution Imager image, with a total live time of $\sim 5 \times 10^4$ s to the source. Overplotted in black are linearly scaled intensity contours of the reconstructed image and the error box from the 1979 March 5 gamma-ray burst.

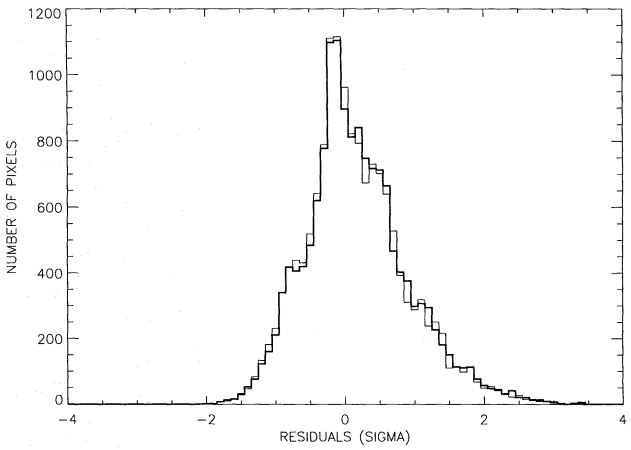

FIG. 2.—Histogram of the residuals from the pixon image reconstruction (*heavy line*) and the unconstrained reconstruction (*thin line*), plotted as functions of the expected value of sigma derived from the model. The residuals were calculated in both cases for the regions of the images containing the just the N49 nebula.

counting rate of RX J05260.3−660433 over the sum of the diffuse nebular emission and the instrumental background was obtained by taking background counts from a circular region of radius 6″ at the center of N49 and subtracting this from the total counts from a similar circular region centered on the position of RX J05260.3−660433. This background region was selected because it more accurately represents the nebular component in the hot-spot region than an annular background taken around the hot spot itself, which would likely include regions free of nebular emission at the northern edge of the N49 image. The fluxes obtained are therefore more conservative than those obtained by Rothschild et al. (1994). The two-dimensional Gaussian fitting procedure was not used to determine the flux for the hot spot because of the large uncertainty introduced in fitting the individual observations. The hot-spot counting rate obtained by the fitting method was, however, consistent with the rate obtained by background subtraction at the 1 σ level. The background subtracted count rates for both RX J05260.3−660433 and the entire N49 nebula are given in Table 1.

To test for variability of the hot-spot point source on the timescale of months to years, the χ^2 statistic can be used to compare the counting rate for all the observations to a constant counting rate model. To minimize effects due to different instrumental responses between the four observations, the ratio between the hot-spot flux $F_{\rm hot}$ and the total nebular flux $F_{\rm neb}$ was used in this calculation. This normalization was possible because the ratio of the hot spot to the nebular flux was small (~2%), and therefore any time variation of the nebular flux was independent of the variation of the hot-spot counting rate. The values of $F_{\rm hot}/F_{\rm neb}$ for each observation are plotted as a function of time in Figure 3. Calculation of χ^2 of the four data points for a constant model equal to the average value of $F_{\rm hot}/F_{\rm neb}$ (0.02) gives a value of 2.34 for 3 degrees of freedom, corresponding to a probability $P(\chi^2 > 2.34)$ of ~50%. Thus, we cannot rule out a constant counting rate from the source RX J05260.3−660433 over the ~2 yr observing period of the *ROSAT* observations of this source. From the values of $F_{\rm hot}/F_{\rm neb}$ we calculate $\sigma_{\rm rms} \sim 0.003$, and the 2 $\sigma_{\rm rms}$ upper limit to variability in the hot spot is ~30% of its mean counting rate.

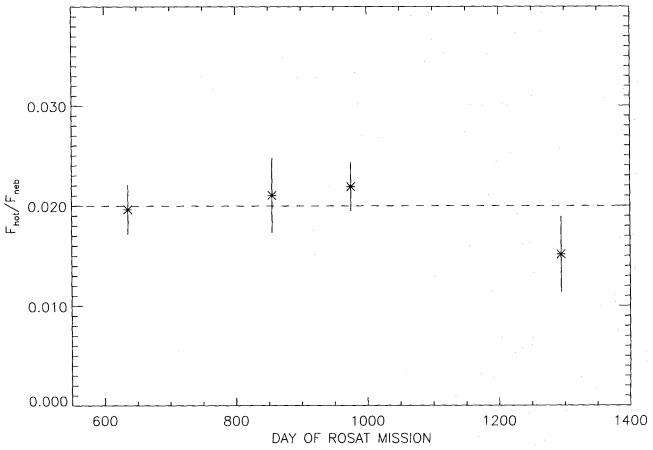

FIG. 3.—Ratio of the hot spot to total nebular flux $F_{\rm hot}/F_{\rm neb}$ is shown plotted as a function of time for the four *ROSAT* observations of N49. The dashed line represents the average of the four ratios used in testing for variability.

Although the HRI has limited spectral capability, the unabsorbed luminosity of the X-ray point source RX J05260.3−660433 can be calculated from the detector response by assuming a spectral shape and a distance to the source. The interstellar absorption-corrected blackbody luminosity $L_{\rm black}$ and the power law luminosity $L_{\rm pwr}$ were calculated assuming a blackbody temperature of $\sim 1.2 \times 10^6$ K or a photon index of −2.2 with a neutral hydrogen column density along the line of sight of $5\text{–}10 \times 10^{21}$ atoms cm^{-2} (Ögelman 1995, private communication). Here the blackbody temperature corresponds to the surface temperature (at ∞) of a 5400 yr neutron star of radius 10 km and mass 1.4 $M_\odot$, assuming pure modified Urca process cooling with no exotic cooling mechanisms or superfluidity (see Fig. 1 of Page & Applegate 1992). The power-law photon index is from the *ASCA* measurement of the spectrum of AX 1805.7−2025, the quiescent X-ray counterpart to SGR 1806−20 (Murakami et al. 1994). Using the average RX J05260.3−660433 counting rate of 0.016 counts s^{-1} and a distance of 49 kpc to N49, we obtain the unabsorbed 0.1–2.4 keV luminosities given in Table 2. Extrapolation of the power-law models to higher energies yields 2–10 keV luminosities of $4\text{–}9 \times 10^{35}$ ergs s^{-1}, which is factor of ~1.5 more than the *ASCA* result for AX 1805.7−2025. The 0.1–2.4 keV luminosity of the hot-spot point source is also ~2–6 times less than the luminosity of the Crab Nebula in the same energy band (Harnden & Seward 1984).

Optical images of N49 in O III and 6100 Å were obtained (Vancura et al. 1992) and compared to both the smoothed X-ray image and the reconstructed image. Figure 4 shows the O III (*a*) and 6100 Å (*b*) images of N49, with the X-ray contours from the pixon reconstructed image overplotted. In the both optical images, little significant flux is evident in the region of RX J05260.3−660433, while the southeast region contains flux that is well correlated with the X-ray emission.

An upper limit for stellar emission in the RX J05260.3−660433 error circle can be obtained by comparing the maximum point source flux in the error circle with the flux of a reference star. Using star 3 from Fishman, Duthie, & Dufour (1981), we derive a lower limit in visual magnitudes of $m_V \sim 21$ for a stellar point source in the best-fit error box for the X-ray hot spot. By using the relation between neutral hydrogen column density and color excess for the LMC (Koornneef 1982) and an extinction curve (Savage & Mathis 1979), we derive ~1.5 mag of visual extinction in the direction of RX J05260.3−660433. At the distance of the LMC, the lower limit in absolute

TABLE 2

UNABSORBED X-RAY LUMINOSITY OF THE N49 HOT-SPOT SOURCE

Model	L_5 (ergs s^{-1})	L_{10} (ergs s^{-1})
Power Law.....	1×10^{36}	3×10^{36}
Blackbody.....	6×10^{36}	3×10^{37}

NOTE.—The power-law photon index and blackbody temperature were taken to be −2.2 and 1.2×10^6 K, respectively. L_5 and L_{10} are the luminosities for $N_{\rm H}$ values of 5×10^{21} cm^{-2} and 10×10^{21} cm^{-2}. The distance to the source was assumed to be 49 kpc.

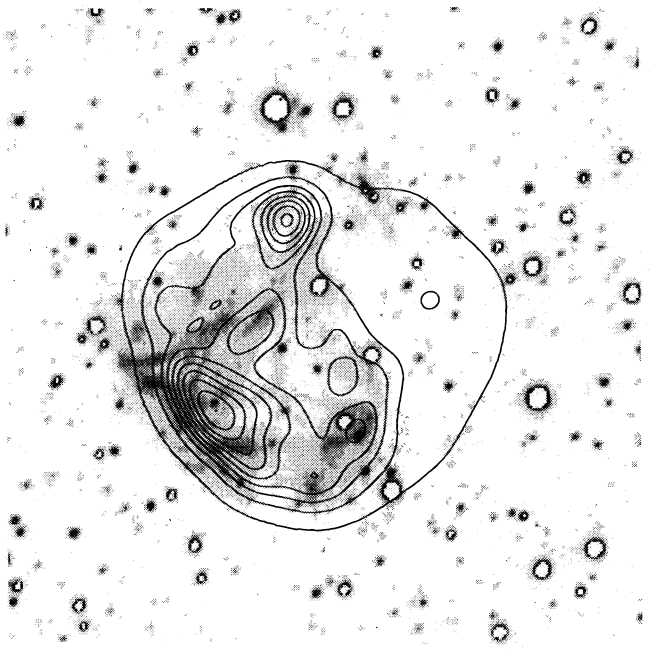

FIG. 4a

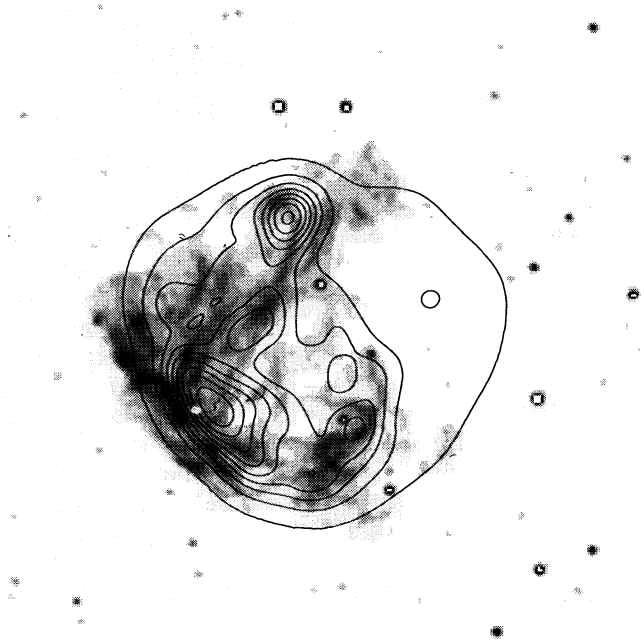

FIG. 4b

FIG. 4.—6100 Å (*top*) and O III (*bottom*) images of N49 with the linearly scaled contours from the reconstructed X-ray image overplotted. The optical images have been overexposed to enhance the faint emission.

magnitudes is $M_V \sim 1$, or no stellar companion more massive than a main-sequence star of spectral type A0.

3. TIMING ANALYSIS

The X-ray emission from the hot spot was searched for coherent pulsations in the period range from 7.5–8.5 s, corresponding to the periodicity detected during the 1979 March 5 gamma-ray burst from SGR 0526−66 (Mazets et al. 1979). For each data set, the arrival times of photons were taken from a circular region of radius 6′ centered on the best-fit position for RX J05260.3−660433. All arrival times were corrected to the solar system barycenter. Because of the presence of significant gaps in the data stream, the data was analyzed using the summed or incoherent FFT method in which fast Fourier transforms are performed on segments of the data, and the power spectra are coadded. This procedure avoids the problem of spurious features appearing in the power spectrum at low frequencies due to data gaps and avoids the software problems associated with the use of a single (long) time series.

To maximize the sensitivity of the analysis, the four *ROSAT* observations were treated as a single data set. This can be done because the effect of frequency smearing in the periodic signal from a putative neutron star, between observations, is small for the frequency resolution and period range of interest. The frequency shift between two observations separated by a time T is given by $\Delta f = -T\dot{P}/P^2 \sim 2.3 \times 10^{-5}$ s^{-1}, where the period derivative $\dot{P} = 0.5P/t \sim 2.35 \times 10^{-11}$. Here t is the age of the pulsar (5400 yr), $T = 2$ yr, and we have assumed that the initial spin period was much less than 8 s (Manchester & Taylor 1981). To maximize the data usage, the length of each time stretch for the FFTs was chosen to be ~600 s, yielding 54 FFT segments for the total power spectrum. The total power spectrum obtained this way from RX J05260.3−660433 is shown in Figure 5*a*.

The dotted lines in Figure 5 represent the power levels corresponding to the indicated probability of the noise power reaching that level in a single frequency bin given the number of frequencies examined. This assumes Poisson noise and does not include noise due to instrumental effects. For the total power spectrum the probability distribution of the noise power for a single frequency bin is given by the χ^2 distribution for $2n$ degrees of freedom, where n is the number of power spectra added together. The probability P of getting a noise power p or greater for N frequency bins is then given by $P = 1 - [1 - Q(\chi^2 \mid 2n)]^N$, where $Q(\chi^2 \mid 2n)$ is the integral of the χ^2 distribution (Van der Klis 1989):

$$Q(\chi^2 \mid 2n) = [2^n \Gamma(n)]^{-1} \int_p^\infty t^{n-1} e^{-t/2}\, dt \,. \qquad (1)$$

The sensitivity of the FFT analysis was tested by performing an identical analysis on simulated pulsar data sets with the same total count rate and data gap structure as the observations. The number of counts contained in each data interval of the simulation was obtained by taking Poisson deviations from the expected (average) count rates. The expected count rate was modeled as a constant rate plus a periodic component. Each simulated pulse profile was modeled as a simple square wave characterized by a broad duty cycle (0.5), an initial period of 8 s, and a period derivative of $\dot{P} = 2.35 \times 10^{-11}$. The fraction of pulsed photons in the simulation was then varied until a peak in the total power spectrum corresponding to a small noise probability $P < 0.01$ was produced. It is worth noting that although $\dot{P}$ was used in the simulation, the effect of frequency smearing was small for the frequency range of interest. For each simulation, the total counting rate was held fixed at 0.034 counts

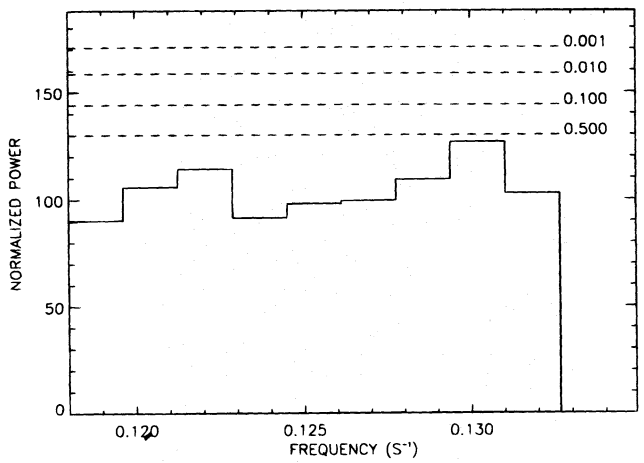

FIG. 5*a*

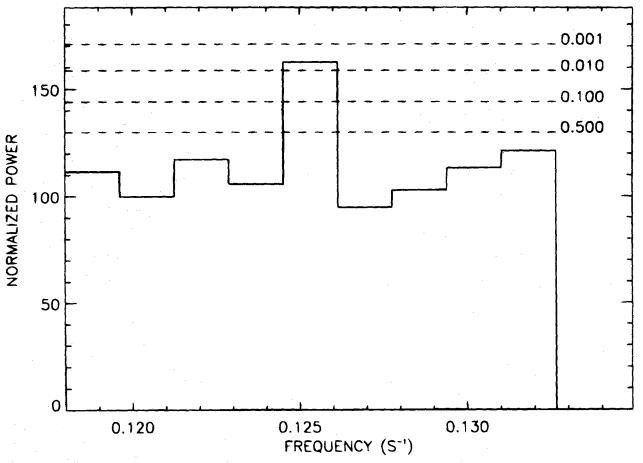

FIG. 5*b*

FIG. 5.—Total power spectrum from both RX J05260.3−660433 (*left*) and a simulated pulsar (*right*) for periods from 7.5 to 8.5 s. The power spectra represents the sum of 54 individual power spectra of length 614 s and time resolution 0.6 s, taken from all four *ROSAT* observations (*left*) and from a simulated pulsar with the same total count rate and a pulsed fraction of 31% (*right*). The values on the right are the probabilities of obtaining the indicated total power levels in a single frequency bin, given pure Poisson noise and the number of frequencies examined.

s^{-1}, the mean total (source + background) counting rate of the data sets centered on RX J05260.3−660433. The minimum detectable pulse fraction for the simulated pulsar data sets was 31%, yielding an upper limit on the source pulsed fraction of photons from RX J05260.3−660433 of 66%. The power spectrum corresponding to this minimum, simulated, pulsed fraction is shown in Figure 5 (*bottom*).

Because of the "diluting" effect of the high nebular background counting rate and the statistical penalty in calculating P for many frequencies (large N), the simulations indicated that the present observations were insensitive to broadband periodicity searches. Also contributing to this is the fact that the data sets cannot be safely combined at high frequencies because of the dependence of frequency smearing on frequency ($\Delta f \propto f^2$). In this case the pulsed fraction required for detection in the simulated pulsar data sets is greater than the fraction of photons from RX J05260.3−660433 in the *ROSAT* data sets. Consequently any attempt to derive an upper limit for the pulsed fraction from the source for periods less than ~8 s was not useful.

4. DISCUSSION

Examination of both the smoothed and reconstructed X-ray images of N49 reveal the hot-spot X-ray morphology to be unlike that of the other emission components in the nebula. The brightest feature of the nebula is the ridgelike feature in the southeast quadrant, where the supernova blast wave appears to be interacting with a dense portion of the interstellar medium, or possibly with a molecular cloud (Hughes, Bronfman, & Nyman 1989). The subsequent X-ray emission is caused by thermal bremsstrahlung of electrons from H and He ions collisionally ionized in the gas heated by the supernova shockwave (Spitzer 1978, p. 8). Heavier species such as O III are also ionized and emit the line radiation seen in the optical images as they recombine behind the shock. The broadband 6100 Å image is dominated by stellar continuum radiation but also contains appreciable amounts of recombination continuum radiation (both 1 and 2 photon) from hydrogen and helium that also results from shock processes (see Vancura et al. 1992, § 3.3.2). Thus, the correlation seen between the optical and X-ray emissions in the southeastern quadrant of N49 is consistent with a common physical origin of the emission.

The hot-spot morphology is seen to be very different from that of the southeast emission ridge. In the reconstructed X-ray image the hot spot appears as a fuzzy "bump" superimposed on a broad plateau of nebular emission bounded on the southeastern edge by a bright shell. The morphology of this source appears asymmetrical, with steeper X-ray gradients on the northern half of the hot spot and a slight cometlike tail extending toward the center of the nebula. The morphology of the source is not shell-like, but bloblike, and oriented such that the long axis is perpendicular to the direction of the supernova blast wave. The possibility that the X-ray hot spot represents a small cloud overrun by the supernova shockwave is suggested by the bloblike morphology. But this hypothesis is apparently ruled out by the lack of O III and continuum emission from the region, which has been seen in other such interactions (Graham et al. 1995). The shape of the hot-spot source is also contrary to what one might expect from a cloud/blast wave interaction. Both the smoothed X-ray image and the reconstructed image suggest extension of the source in a direction perpendicular to the supernova shock front, while theoretical models indicate that cloud expansion from shock encounters should occur primarily in an axial direction, parallel to the shock (Klein, McKee, & Colella 1989).

If the X-ray hot spot is not associated with the supernova shock, it could represent material ejected in the supernova explosion: either fragments of the progenitor star core or the neutron star itself. As noted in Rothschild et al. (1994), the transverse velocity implied by the angular offset of the source from the center of the nebula is ~1200 km s^{-1}, depending on the point one takes for the origin of the explosion. This is similar to the mean velocity of fragments observed in the Vela supernova remnant, a 10^4 yr remnant also observed by *ROSAT* (Aschenbach, Egger, & Trümper 1995). The brightest of these Vela "shards," however, has a soft X-ray luminosity of $L_X \sim 10^{33}$ erg s^{-1}, which is a factor of ~1000 less than the luminosity of the N49 hot spot. If the

N49 hot spot is a fragment from the supernova progenitor, we would also expect to see other fragments (point sources) in the X-ray image of the nebula, which we do not.

If the N49 hot-spot source is the neutron star ejected in the supernova explosion, the high transverse velocity implied by the angular offset of this object would place it near the high end of the distribution of radio pulsar velocities (Lyne & Lorimer 1994). The high velocity of RX J05260.3−660433 may not be improbable, however, in light of recent work which suggests that there may be a large population of high-velocity neutron stars that are undetected due to selection effects (Cordes, Chernoff, & Wasserman 1995). Because this velocity exceeds the velocities imparted during normal binary dynamical evolution (Van Paradijs & White 1995), scenarios involving "kick" velocities imparted to the nascent neutron star are favored. A promising model for this involves hydrodynamic forces generated by asymmetries in the collapse and convective "boiling" phase of the supernova explosion (Burrows & Hayes 1995), although three-dimensional simulations have not been performed to show that this method can produce the required velocities (~ 1000 km s^{-1}). A neutron star kick via the radiation reaction force from a misaligned dipole magnetic field in the early stages of the neutron star's life has also been studied (Tademaru & Harrison 1975).

The effective radius of the emitting region $R_{\rm eff}$ can be found by relating the observed X-ray luminosity to the product of the blackbody flux and the emitting area. If we assume that the X-ray spectrum from RX J05260.3−660433 has a blackbody shape with an effective temperature of $T_{\rm eff}$, and that the emission is isotropic, the unabsorbed X-ray luminosity is given by:

$$L_{\rm X}^{u} = 8\pi^2 R_{\rm eff}^2 \frac{h}{c^2}\left(\frac{kT_{\rm eff}}{h}\right)^4 \int_{x_1}^{x_2} \frac{x^3}{e^x - 1}\, dx\,. \qquad (2)$$

Here x_1 and x_2 are the upper and lower energy limits to the *ROSAT* bandpass normalized to $kT_{\rm eff}$, and $L_{\rm X}^{u}$ is the unabsorbed source luminosity as seen by *ROSAT*. The integral in equation (2) can be done numerically, and the equation then gives a value of $R_{\rm eff} = 2000$–5000 km, assuming $T_{\rm eff} = 1.2 \times 10^6$ K, $N_{\rm H} = 5$–10×10^{21} atoms cm^{-2}, and the blackbody luminosity of 6–30×10^{36} ergs s^{-1} obtained from the *ROSAT* observation. This greatly exceeds the range of expected neutron star radii ($\sim$10–20 km), indicating that the neutron star is much hotter than predicted from cooling theory (Page & Applegate 1992), if the spectrum is pure blackbody emission from the surface. We calculate that an effective temperature of ~ 2–5×10^7 K will self-consistently account for the observed *ROSAT* flux (assumed blackbody) and produce an effective emitting radius of 10–20 km. This temperature range is a factor of $\sim$20 greater than predicted for cooling neutron stars, suggesting that reheating must have taken place if the X-ray emission is due to surface blackbody emission.

Information on the spectrum of RX J05260.3−660433 can be ascertained by examining archival images of N49 obtained from the *Einstein* High Resolution Imager data archive. The *Einstein* HRI had an effective energy range (0.14–3.50 keV) that extended to higher energies than the *ROSAT* HRI (see Fig. 6), allowing spectral information to be extracted by comparing count rates obtained from the two different instruments, assuming that the overall flux from the source is constant. N49 was observed twice by the *Einstein* HRI between 1979–1981, with a total live time of $\sim 1.75 \times 10^4$ s. These images were aligned with the *ROSAT* images, and the background-subtracted count rates for RX J05260.3−660433 were obtained for the two observations in the same manner as with the *ROSAT* data. This yielded counting rates of 0.0025 ± 0.0015 and 0.0043 ± 0.0016 counts s^{-1} for the two observations of X-ray hot spot, corresponding to a mean value of 0.003 ± 0.001 counts s^{-1}.

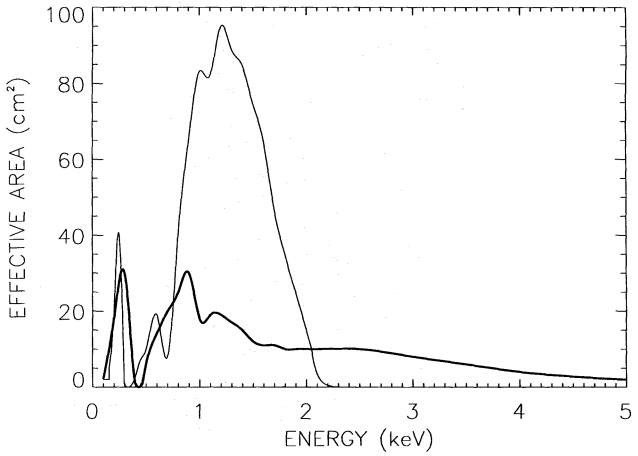

FIG. 6.—Effective area vs. incident photon energy for the *ROSAT* HRI (*thin line*; David et al. 1992) and *Einstein* HRI (*thick line*; Garcia et al. 1990).

To get an indication of the spectral shape that is consistent with both the *ROSAT* and *Einstein* observations of RX J05260.3−660433, we first constructed a grid of power-law and blackbody spectral models by varying, respectively, the photon power-law index Γ or the blackbody temperature $T_{\rm eff}$ for the two models. The column density was held fixed at either 5×10^{21} or 1×10^{22} atoms cm^{-2} for each model. The software package PIMMS was used to adjust the (single) parameter of each model until the resultant counting rate agreed with the mean *ROSAT* count rate of RX J05260.3−660433. These models were then folded through the *Einstein* HRI detector response, producing a count rate that was then checked for consistency with the observed mean *Einstein* count rate from RX J05260.3−660433. For the blackbody models, surface temperatures in the range $T_{\rm eff} \sim 1$–5×10^6 K result in count rates which agree with the *Einstein* observations, but result in emitting radii of 40–5000 km, larger than that of a neutron star. For the power-law models, a range of photon power-law indices $2 \leq \Gamma \leq 5$ is required for consistency between the two observations.

A possible explanation for the X-ray emission from RX J05260.3−660433 is that it is magnetospheric in origin, as in the plerion models for the quiescent X-ray and radio emission from SGR (Rothschild et al. 1994; Harding 1995). Plerions are compact synchrotron nebulae surrounding and powered by neutron stars. The known plerions have power-law spectra characterized by a photon index $0.6 \leq \Gamma \leq 1.5$ (Seward & Wang 1988), which is harder than the power-law spectrum of RX J05260.3−660433 allowed by the combined *ROSAT* and *Einstein* analysis described above. However, an object with a power-law spectrum similar to SGR 1806−20 ($\Gamma \sim 2.2$; Murakami et al. 1994) is permitted by the present observations.

Because the ultimate energy source of plerions is believed to be the rotational energy of the constituent neutron star, the minimum rotation rate can be constrained by the X-ray luminosity of the plerion. This can be seen by expressing the observed X-ray luminosity L_X in terms of the spin down luminosity $\dot{E}$ and an efficiency factor η:

$$L_X = \eta \dot{E} = 5.4 \times 10^{33} \eta \left(\frac{P}{8s}\right)^{-2} \times \left(\frac{I_{ns}}{3 \times 10^{45}\ g\ cm^2}\right)\left(\frac{t}{5400\ yr}\right)^{-1} \text{ergs s}^{-1}. \quad (3)$$

Here I_{ns} is the moment of inertia of a neutron star, and we have made the assumption that the timing age t of the pulsar is equal to the age of N49 and is given by $t = 0.5P/\dot{P}$ (Manchester & Taylor 1981). Equation (3) indicates that an $\sim$8 s spin period is insufficient to power a nonthermal nebula around the quiescent counterpart to SGR 0525−66 ($\eta > 1$). If, however (as pointed out by Rothschild et al. 1994), the 23 ms quasi-periodic oscillation (QPO) detected from SGR 0526−66 during the March 5 event is the neutron star rotation period, the energetics requirement of the plerion model are easily met ($\eta \sim 10^{-4}$). Detection of a pulsar period in RX J05260.3-660433 would clearly help constrain this model. This could possibly be accomplished with the PCA and HEXTE instruments on board the *Rossi X-ray Timing Explorer* that have high sensitivities in the 2–250 keV (combined) band due to a combination of large effective area and timing accuracy.

Similarities between the lightcurves of SGR bursts and Type II X-ray bursts from some low-mass X-ray binaries (LMXRB) has prompted the suggestion that these two types of objects may be related (Thompson & Duncan 1995). The binary hypothesis is attractive because it offers a simple source of energy for both quiescent and burst emission from SGR: accretion of matter from the primary on to the neutron star. If this scenario were true, however, it would suggest that the X-ray point source is not, in fact, associated with N49 because the energy required to accelerate even a low-mass binary system to speeds greater than 1000 km s^{-1} approaches the entire kinetic energy budget of a typical supernova explosion. Nonetheless, the optical flux expected from RX J05260.3−660433 if it were an LMXRB system can be estimated from the relationship between the optical and X-ray fluxes for these systems (Van Paradijs 1995). Using a blackbody model with $T_{eff} = 4 \times 10^6$ K and $N_H = 1 \times 10^{22}$ yields a 2–11 keV flux of 3×10^{-13} ergs cm^{-2} s^{-1} for RX J05260.3−660433, given the mean *ROSAT* HRI counting rate (0.1–2.4 keV). This corresponds to an observed optical flux of $\sim 1.5 \times 10^{-10}$ ergs cm^{-2} s^{-1}, or an absolute visual magnitude of $M_V \sim -9$, given a distance of 49 kpc to the LMC. This is much less (brighter) than the optical upper limit of $M_V \sim 1$ for point sources in the positional error box of RX J05260.3−660433, indicating that a typical LMXRB would have been seen in the optical images of this region. In addition, the lack of variability of RX J05260.3−660433 is unlike LMXRBs, which often have flaring episodes in which the source flux increases by factors of $\sim$5 over timescales of a few days (Stewart et al. 1991). More sensitive optical exposures are required, however, to rule out the existence of a low mass ($\sim$M star) stellar companion in the RX J05260.3−660433 error box.

The upper limit on the pulsed fraction of 66% does not rule out a standard soft X-ray pulsar as the origin of the RX J05260.3−660433 emission as the pulsed fraction for these sources is typically $\sim$10%–30% (Ögelman 1995). This upper limit is also greater than the 50–200 keV pulsed fraction ($\sim$50%) seen from SGR 0526−66 during the 1979 March 5 burst (Mazets et al. 1979).

5. CONCLUSION

The present *ROSAT* observations of N49 have isolated the position of the soft X-ray hot spot that has been proposed to be the counterpart to the extraordinary 1979 March 5 gamma ray burst to within 5″, yet examination of optical images of the error box failed to find significant optical emission in this region. This implies that the X-ray emission from the counterpart source RX J05260.3−660433 is not due to "normal" supernova emission processes. No evidence for variability on a timescale of months to years was found, and we find that the soft X-ray luminosity of the hot-spot source is greater than the expected luminosity of thermal emission from the surface of a neutron star of the same age as N49. This lack of long term temporal variability argues against the accreting X-ray binary hypothesis for the hot-spot source. Assuming no long term temporal variability of the source, a "hardness" test using archival *Einstein* data favors a softer X-ray spectrum than observed for known plerions, but does not rule out a spectrum similar to that observed for SGR 1806−20. A search for evidence of pulsations at the observed period of the March 5 event turned up negative. Clearly more observations of this source with instruments having arcsecond spatial resolution and spectral capability (e.g., AXAF) are needed to ascertain the shape of the X-ray spectrum, and deeper observations with greater sensitivity are needed to search for pulsations.

We would like to thank Lyle Ford and anonymous referees for useful comments and discussions, and Hakki Ögelman, John Dickel, and Rob Petre for samples of their data in advance of publication. We also thank the duty scientists at the *ROSAT* Science Data Center for help with the *ROSAT* data, and Gail Reichert for her IDL software and assistance. This research was supported by NASA contracts NAS 5-30720 and NAGW-1970.

REFERENCES

Aschenbach, B., Egger, R., & Trümper, J. 1995, Nature, 373, 587
Barat, C., et al. 1983, A&A, 126, 400
Burrows, A., & Hayes, J. 1995, in High Velocity Neutron Stars, ed. R. E. Rothschild & R. E. Lingenfelter (New York: AIP), 25
Cline, T. L., et al. 1982, ApJ, 255, L45
Cordes, J. M., Chernoff, D. F., & Wasserman, I. 1995, in High Velocity Neutron Stars, ed. R. E. Rothschild & R. E. Lingenfelter (New York: AIP Press), 11
David, L. P., Harnden, F. R., Kearns, K. E., & Zombeck, M. V. 1992, in The *ROSAT* Data Products Guide, US *ROSAT* Science Data Center Pub.
Dickel, J. R., et al. 1995, ApJ, 448, 623
Dixon, D. D., Tümer, O. T., Kurfess, J. D., Purcell, W. R., Piña, R. K., & Puetter, R. C. 1996, ApJ, in press
Duncan, R. C., & Thompson, C. 1992, ApJ, 392, L9
Feast, M. W. 1991, in The Magellanic Clouds, ed. R. Haynes & D. Milne (Dordrecht: Kluwer), 1
Fishman, G. J., Duthie, J. G., & Dufour, R. J. 1981, Ap&SS, 75, 135
Garcia, M. R., et al. 1990, in The *Einstein* Observatory Database of HRI X-Ray Images (CD-ROM booklet), Smithsonian Institution Astrophysical Observatory
Graham, J. R., Levenson, N. A., Hester, J. J., Raymond, J. C., & Petre, R. 1995, ApJ, 444, 787

Harding, A. K. 1995, in High Velocity Neutron Stars, ed. R. E. Rothschild & R. E. Lingenfelter (New York: AIP), 118
Harnden, F. R., & Seward, F. D. 1984, ApJ, 283, 279
Hughes, J. P., Bronfman, L., & Nyman, L. 1989, in Supernovae, ed. S. E. Woosley (New York : Springer), 679
Klein, R. I., McKee, C. F., & Colella, P. 1989, in Supernovae, ed. S. E. Woosley (New York : Springer), 679
Koornneef, J. 1982, A&A, 107, 247
Kulkarni, S. R., & Frail, D. R. 1993, Nature, 365, 33
Lyne, A. G., & Lorimer, D. R. 1994, Nature, 369, 127
Manchester, R. N., & Taylor, J. H. 1981, AJ, 86, 1961
Mazets, E. P., Golenetskii, S. V., Ilinskii, V. N., Aptekar, R. L., & Guryan, Yu. A. 1979, Nature, 282, 587
Murakami, T., Tanaka, Y., Kulkarni, S. R., Ogasaka, Y., Sonobe, T., Ogawara, Y., Aoki, T., & Yoshida, A. 1994, Nature, 368, 127
Norris, J. P., Hertz, P., Wood, K. S., & Kouveliotou, C. 1991, ApJ, 366, 240
Ögelman, H. 1995, in The Lives of Neutron Stars, ed. M. A. Alpar, Ü. Kiziloğlu, & J. van Paradijs (Dordrecht: Kluwer), 101
Page, D., & Applegate, J. H. 1992, ApJ, 394, L17
Puetter, R. C. 1994, Proc. SPIE, 2302, 112
Rothschild, R. E. 1995, in High Velocity Neutron Stars, ed. R. E. Rothschild & R. E. Lingenfelter (New York : AIP), 51
Rothschild, R. E., Kulkarni, S. R., & Lingenfelter, R. E. 1994, Nature, 368, 432
Rothschild, R. E., Lingenfelter, R. E., Seward, F. D., & Vancura, O. 1993, in Compton Gamma-Ray Observatory, ed. M. Freidlander, N. Gehrels, & D. J. Macomb (New York: AIP), 808
Savage, B. D., & Mathis, J. S. 1979, AR&A, 17, 73
Seward, F. D., & Wang, Z. 1988, ApJ, 332, 199
Spitzer, L. 1978, Physical Processes in the Interstellar Medium (New York: Wiley)
Stewart, R. T., Nelson, G. J., Pennix, W., Kitamoto, S., Miyamoto, S., & Nicolson, G. D. 1991, MNRAS, 253, 212
Tademaru, E., & Harrison, E. R. 1975, Nature, 254, 676
Tanaka, Y. I. 1993, IAU Circ. 5880
Thompson, C., & Duncan, R. C. 1995, MNRAS, 275, 255
Vancura, O., Blair, W. P., Long, K. S., & Raymond, J. C. 1992, ApJ, 394, 158
Van der Klis, M. 1989, in Timing Neutron Stars, ed. H. Ögelman & E. P. G. van den Heuvel (Dordrecht: Kluwer), 27
Van Paradijs, J. 1995, in The Lives of the Neutron Stars, ed. M. A. Alpar, Ü. Kiziloğlu, & J. van Paradijs (Dordrecht: Kluwer), 281
Van Paradijs, J., & White, N. 1995, ApJ, 447, 33
Vasisht, G., Kulkarni, S. R., Frail, D. A., & Greiner, J. 1994, ApJ, 431, L35